

ON THE USE OF RISK MEASURES IN DIGITAL TWINS TO IDENTIFY WEAKNESSES IN STRUCTURES

FACUNDO N. AIRAUDO, HARBIR ANTIL, RAINALD LÖHNER, AND UMARKHON RAKHIMOV

ABSTRACT. Given measurements from sensors and a set of standard forces, an optimization based approach to identify weakness in structures is introduced. The key novelty lies in letting the load and measurements to be random variables. Subsequently the conditional-value-at-risk (CVaR) is minimized subject to the elasticity equations as constraints. CVaR is a risk measure that leads to minimization of rare and low probability events which the standard expectation cannot. The optimization variable is the (deterministic) strength factor which appears as a coefficient in the elasticity equation, thus making the problem nonconvex. Due to uncertainty, the problem is high dimensional and, due to CVaR, the problem is nonsmooth. An adjoint based approach is developed with quadrature in the random variables. Numerical results are presented in the context of a plate, a large structure with trusses similar to those used in solar arrays or cranes, and a footbridge.

1. INTRODUCTION

Given that all materials exposed to the environment and/or undergoing loads eventually age and fail, the task of trying to detect and localize weaknesses in structures is common to many fields. To mention just a few: airplanes, drones and missiles, turbines, launch pads and airport infrastructure, wind turbines, satellites and space stations. Traditionally, manual inspection was the only way of carrying out this task, aided by ultrasound, X-ray, or vibration analysis techniques. The advent of accurate, abundant and cheap sensors, together with detailed, high-fidelity computational models in an environment of digital twins has opened the possibility of enhancing and automating the detection and localization of weaknesses in structures. The authors in article [1] introduced an adjoint based optimization approach [11, 17, 8, 5] to identify weakness in structures under the deterministic setting. Given the displacement or strain measurements from certain sensor measurements, the goal is to solve an inverse problem to determine material properties. This amounts to minimizing a cost functional subject to elasticity equations as constraints, and is a deterministic optimization problem with partial differential equations (PDE) as constraints. Here the optimization problem itself can be thought as a ‘digital twin’ which is informed by the physical system via sensor measurements. The digital twin then make predictions about the structural weakness.

However, the underlying elasticity equation contains various unknown quantities. In particular, the load measurements can present uncertainty, especially if it comes from sources that were not accounted for, like wind or temperature variations. In addition, the measurements from sensors could be faulty due to sensor errors or various signal-to-noise thresholds. The present article proposes to model these quantities as random fields. This has dual benefits: firstly, one can tackle the unknown quantities and secondly, it will lead to designs which are resilient to uncertainty. However, several challenges appear. Due to random data/inputs,

the PDE solution becomes a random field and the cost functional becomes a random variable. It is unrealistic to minimize a random variable. Moreover, these problems can be very high dimensional problems.

Traditionally, cost functionals that are random variables have been handled by computing their expectation. However, evaluating the expectation is like computing an average. This scenario cannot handle the outliers which lie in the tail of a distribution. Instead, following [15], we consider the so-called conditional-value-at-risk (CVaR), which is the average of the β -tail of the distribution with $\beta \in (0, 1)$. The first use of CVaR in optimization problems with PDE constraints can be found in [10]. Recently, this approach has been further extended using tensor decomposition tools [3] to tackle higher dimensional problems. See also [4] for a tensor-train framework with state constraints (e.g., constraints on the displacement).

Outline: The remainder of the paper has been organized as follows: In section 2 we state the well known definition of CVaR. Section 3 focuses on the optimization problem with elasticity constraints under uncertainty. Section 4 discusses the adjoint formulation to evaluate the gradients. Section 5, presents our implementation details and various numerical examples. Finally, in section 6 a few concluding remarks are provided.

2. CONDITIONAL VALUE AT RISK

Let $\mathcal{L} := (D, \mathcal{A}, \mathbb{P})$ be a complete probability space. Here D denotes the set of outcomes, $\mathcal{A} \subset 2^D$ is the σ -algebra of events, and $\mathbb{P} : \mathcal{A} \rightarrow [0, 1]$ is the appropriate probability measure. Consider a scalar random variable X defined on \mathcal{L} . In our setting below, X will be the random variable objective function. The expectation of X is given by

$$\mathbb{E}[X] = \int_D X(\omega) d\mathbb{P}(\omega). \quad (1)$$

X can be, for example, a typical objective function in an optimization problem, minimizing its standard expectation would be regarded as a risk neutral approach. Making use of risk measures like CVaR_β allow the optimization process to focus on certain areas of the random domain instead of the whole range.

If $\beta \in (0, 1)$ is fixed, and $\mathbb{P}[X \leq t]$ denotes the probability of the random variable X is less than or equal to t , then the value-at-risk (VaR) is given by

$$\text{VaR}_\beta[X] := \inf_{t \in \mathbb{R}} \{t : \mathbb{P}[X \leq t] \geq \beta\}. \quad (2)$$

Unfortunately, VaR_β is not a coherent risk measure as it violates the sub-additivity / convexity axiom in risk-measures [15]. Instead, CVaR_β , which is coherent, is a preferred risk-measure. Due to Rockafellar and Uryasev [13, 14], CVaR_β can be written as

$$\text{CVaR}_\beta[X] = \inf_{t \in \mathbb{R}} \left\{ t + \frac{1}{1 - \beta} \mathbb{E}[(X - t)_+] \right\}, \quad (3)$$

where $(X - t)_+ = \max\{X - t, 0\}$. In case of a continuous random variable, the above definition is equivalent to $\text{CVaR}_\beta[X] = \mathbb{E}[X : X > \text{VaR}_\beta[X]]$, i.e., $\text{CVaR}_\beta[X]$ is indeed the average of β -tail of the distribution of X . Namely, $\text{CVaR}_\beta[X]$ focuses on the rare and low probability events, especially when $\beta \rightarrow 1$. This is further illustrated in Figure 2.1 by the shaded region under the curve. I.e., the Cumulative Distribution Function (CDF)

here is larger than β and here $X > \text{VaR}_\beta[X]$ with probability $1 - \beta$. Notice that the main reason for considering CVaR_β instead of VaR_β is that the latter is not coherent. In addition, the expression of CVaR_β given in (3) making it much more computationally tractable in comparison to VaR_β .

Throughout, we make the finite dimensional noise assumption. We assume that ω can be sampled via a finite random vector $\xi : D \rightarrow \Xi$ instead, where $\Xi = \xi(D) \subset \mathbb{R}^d$ with $d \in \mathbb{N}$. This allows us to redefine the probability space as (Ξ, Σ, γ) where $\Sigma = \xi(\mathcal{A})$ is the σ -algebra and $\gamma(\xi)$ is the continuous probability density function such that $\mathbb{E}[X] = \int_{\Xi} X(\xi) \gamma(\xi) d\xi$. The random variable $X(\xi)$ can be considered as a function of the random vector $\xi = (\xi^{(1)}, \dots, \xi^{(d)})$.

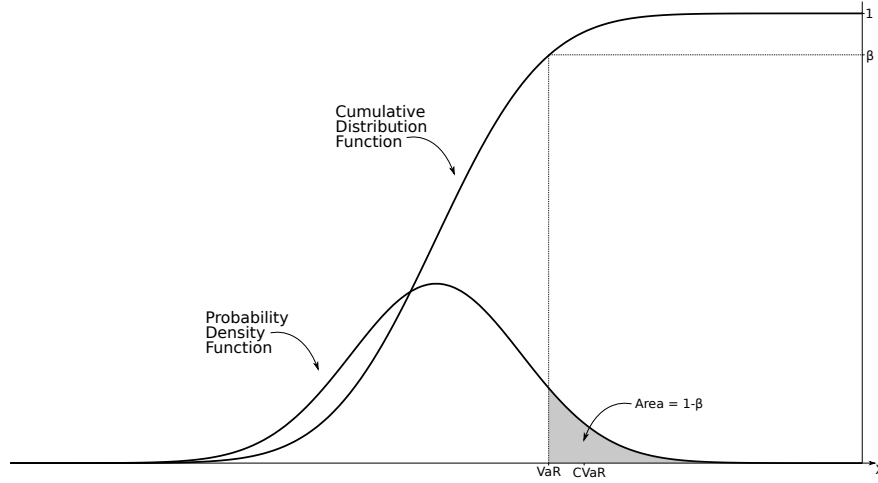


FIGURE 2.1. Illustrations of a normal Probability Density Function (PDF) and its corresponding Cumulative Distribution function (CDF) for a random loss function X . For an arbitrary β , VaR_β and CVaR_β are shown.

3. PROBLEM FORMULATION

In what follows we assume that a spatial discretization has been carried out via finite elements, finite volumes or finite differences, even though the discussion below is independent of any particular discretization. The determination of material properties (or weaknesses) may be formulated as an optimization problem for the deterministic strength factor $\alpha(\mathbf{x})$ as follows: Let the load $\Xi \ni \xi \mapsto \mathbf{f}(\xi)$ be a random vector with known distribution. Moreover, let $\mathbf{x}_j, j = 1, \dots, m$ denotes the m measurement locations for deformations $\Xi \ni \xi \mapsto \mathbf{u}_j^{md}(\xi)$, $j = 1, \dots, m$ or strains $\Xi \ni \xi \mapsto \mathbf{s}_j^{ms}(\xi)$, $j = 1, \dots, m$.

Then the random variable objective functional that we want to minimize to identify the spatial distribution of the strength factor α is given by

$$I(\mathbf{u}(\xi), \alpha) = \frac{1}{2} \sum_{j=1}^m w_j^{md}(\xi) (\mathbf{u}_j^{md}(\xi) - \mathbf{I}_j^d \cdot \mathbf{u}(\xi))^2 + \frac{1}{2} \sum_{j=1}^m w_j^{ms}(\xi) (\mathbf{s}_j^{ms}(\xi) - \mathbf{I}_j^s \cdot \mathbf{s}(\xi))^2, \quad (4)$$

where w_j^{md}, w_j^{ms} are displacement and strain weights possibly depending on parameter ξ , $\mathbf{I}^d, \mathbf{I}^s$ interpolation matrices that are used to obtain the displacements and strains from the finite element mesh at the measurement locations. However, as mentioned earlier, minimizing $I(\mathbf{u}(\xi), \alpha)$ in (5a) is not tractable. We scalarize this using CVaR $_\beta$ given in (3). The resulting minimization problem is given by

$$\inf_{\alpha, t} \left\{ \text{CVaR}_\beta[I(\mathbf{u}(\cdot), \alpha)] := \left\{ t + \frac{1}{1-\beta} \mathbb{E}[(I(\mathbf{u}(\cdot), \alpha) - t)_+] \right\} \right\} \quad (5a)$$

subject to the finite element description (e.g. trusses, beams, plates, shells, solids) of the structure [19, 16] under consideration (i.e. the digital twin/system [12, 6]):

$$\mathbf{K}(\alpha)\mathbf{u}(\xi) = \mathbf{f}(\xi), \quad \text{a.s. } \xi \in \Xi. \quad (5b)$$

Here \mathbf{K} is the usual stiffness matrix, which is obtained by assembling all the element matrices:

$$\mathbf{K} = \sum_{e=1}^{N_e} \alpha_e \mathbf{K}_e, \quad (6)$$

where the strength factor α_e of the elements has already been incorporated. We note in passing that in order to ensure that \mathbf{K} is invertible and non-degenerate $\alpha_e > \epsilon > 0$.

4. ADJOINT APPROACH

In order to establish a gradient based method, we need to calculate the derivative of CVaR $_\beta$ with respect to α . Notice that $(\cdot)_+$ is not differentiable in the classical sense, but it is differentiable in a generalized sense [18, 2]. We set the derivative of $(x)_+$ as

$$(x)'_+ = \begin{cases} 1 & \text{if } x \geq 0 \\ 0 & \text{otherwise,} \end{cases}$$

enabling us to use a gradient based method. If one wants to use a higher order method (like Newton), then one approach is to smooth the $(\cdot)_+$ function [10, 4].

Next, let the Lagrangian functional be

$$\mathcal{L}(\mathbf{u}, \alpha, \tilde{\mathbf{u}}) = \text{CVaR}_\beta[I(\mathbf{u}(\cdot), \alpha)] + \int_{\Xi} \gamma(\xi) \tilde{\mathbf{u}}(\xi)^\top (\mathbf{K}(\alpha)\mathbf{u}(\xi) - \mathbf{f}(\xi)) d\xi$$

where $\tilde{\mathbf{u}}$ indicates the Lagrange multiplier. A variation of \mathcal{L} with respect to \mathbf{u} , at a stationary point, leads to

$$0 = \delta_{\mathbf{u}} \mathcal{L}(\mathbf{u}, \alpha, \tilde{\mathbf{u}}) = \frac{1}{1-\beta} \mathbb{E}[(I(\mathbf{u}(\cdot), \alpha) - t)'_+ \delta_{\mathbf{u}} I(\mathbf{u}(\cdot), \alpha)] + \int_{\Xi} \gamma(\xi) \mathbf{K}(\alpha)^\top \tilde{\mathbf{u}}(\xi) d\xi,$$

which gives rise to the adjoint equation

$$\mathbf{K}(\alpha)^\top \tilde{\mathbf{u}}(\xi) = \frac{-1}{1-\beta} [(I(\mathbf{u}(\xi), \alpha) - t)'_+ \delta_{\mathbf{u}} I(\mathbf{u}(\xi), \alpha)], \quad \text{a.s. } \xi \in \Xi. \quad (7)$$

Subsequently, the variation of \mathcal{L} with respect to α gives us the required derivative with respect to α

$$\delta_\alpha \mathcal{L}(\mathbf{u}, \alpha, \tilde{\mathbf{u}}) = \int_{\Xi} \gamma(\xi) \tilde{\mathbf{u}}(\xi)^\top \mathbf{K}'(\alpha) \mathbf{u}(\xi) d\xi. \quad (8)$$

Finally, the variation with respect to t is given by

$$\delta_t \mathcal{L}(\mathbf{u}, \alpha, \tilde{\mathbf{u}}) = 1 - \frac{1}{1 - \beta} \mathbb{E} [(I(\mathbf{u}(\cdot), \alpha) - t)'_+] . \quad (9)$$

With the expression of the derivatives of \mathcal{L} with respect to α and t , we can now create a gradient based method to solve the optimization problem.

5. IMPLEMENTATION DETAILS AND NUMERICAL EXPERIMENTS

The goal of this section is provide several illustrative experiments. Prior to that, we discuss some missing ingredients. Section 5.1 discusses the appropriate weights to be used in (5a). This is followed by section 5.2 which discusses the appropriate smoothing procedure for the gradients, first introduced in [1]. The article [1] also highlights that this smoothing can be associated with the use of appropriate function space based scalar product. Section 5.3 focuses on the approximation of the expectation \mathbb{E} . The proposed approach is applied to illustrative examples in section 5.4. There examples were computed using our codes for optimization and interfacing, and CALCULIX [7] as our solver for the elasticity equations. CALCULIX is a general, open source finite element code for structural mechanics applications with many element types, material models and options.

5.1. Local Weighting. In this study, we consider the following weights in (5a), and refer to [1] for further scenarios:

$$w_{ij}^{md} = \frac{1}{(\mathbf{u}_{ij}^{md})^2} ; w_{ij}^{ms} = \frac{1}{(\mathbf{s}_{ij}^{ms})^2} ; \quad (10)$$

5.2. Smoothing of Gradients. The gradients of the cost function with respect to α allow for oscillatory solutions. One must therefore smooth or ‘regularize’ the spatial distribution. This happens naturally when using few degrees of freedom, i.e. when α is defined via other spatial shape functions (e.g. larger spatial regions of piecewise constant α). As the (possibly oscillatory) gradients obtained in the (many) finite elements are averaged over spatial regions, an intrinsic smoothing occurs. This is not the case if α and the gradient are defined and evaluated in each element separately, allowing for the largest degrees of freedom in a mesh and hence the most accurate representation. Several types of smoothing or ‘regularization’ are possible, see [1]. All of them start by performing a volume averaging from elements to points:

$$\alpha_p = \frac{\sum_e \alpha_e V_e}{\sum_e V_e} \quad (11)$$

where α_p, α_e, V_e denote the value of α at point p , as well as the values of α in element e and the volume of element e , and the sum extends over all the elements surrounding point p . This work uses the averaging process described next.

Simple Point/Element/Point Averaging. In this case, the values of α are cycled between elements and points. When going from point values to element values, a simple average is taken:

$$\alpha_e = \frac{1}{n_e} \sum_i \alpha_i \quad (12)$$

where n_e denotes the number of nodes of an element and the sum extends over all the nodes of the element. After obtaining the new element values via equation (12) the point averages are again evaluated via equation (11). These two steps are repeated for a number of smoothing steps, which typically are in the range 1-5. This form of averaging is very crude, but works very well in practice.

5.3. Approximation of expectation. The expectation $\mathbb{E}[\cdot]$ in (5a), (8), and (9) is approximated using Gauss quadrature. Unfortunately, the computational complexity in this case is $\mathcal{O}(n^d)$ where n is the number of quadrature points in each random variable direction and d is dimension of the random variables. One can overcome this curse of dimensionality by using tensor-train (TT) decomposition as recently shown in [4, 3]. However, the TT decomposition is not used in the present paper.

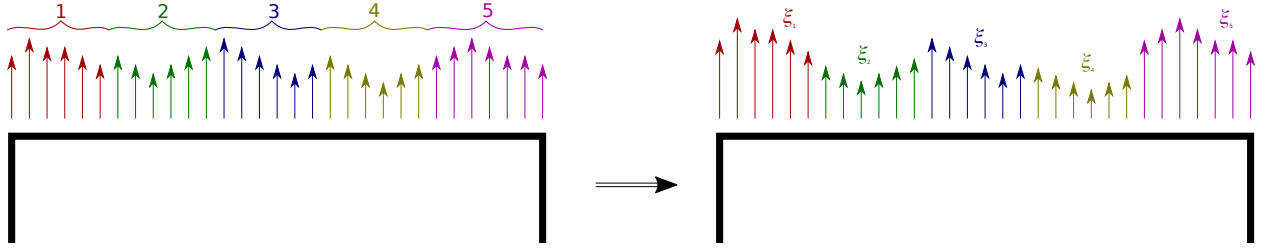


FIGURE 5.1. Illustration of the use of load groups. Each group is scaled by a different random variable ξ_i .

A simpler approach is chosen, in the form of load groups. Since we expect the load to be distributed in space along a certain direction, we divide the load factor into multiple groups, each scaled separately by a random factor. Figure 5.1 shows an example of this concept. The choice of how many groups to use is given by a compromise between required precision and availability of computing resources. In our computations, we choose the groups of uniform width.

For the cases in which a certain degree of uncertainty is expected in the measured loads, we have the following formulation for the forward problem

$$\mathbf{K}(\alpha)\mathbf{u} = \mathbf{Q}_\xi \mathbf{f}, \quad (13)$$

where \mathbf{Q}_ξ is a diagonal matrix that makes it so the load applied to point i is scaled by the proper random variable ξ_{i_g} .

For example, the standard expectation for a continuous random variable from equation (1), rewritten here for clarity:

$$\mathbb{E}[X] = \int_D X(\omega) d\mathbb{P}(\omega).$$

Recalling the finite dimensional noise assumption from section 2, we can rewrite it as

$$\mathbb{E}[X] = \int_{\Xi} X(\xi) \gamma(\xi) d\xi,$$

where ξ is a vector $\xi = (\xi_1, \dots, \xi_{n_l})$ representing the load groups with n_l indicating the number of load groups.

If we discretize the integral using a Gauss quadrature, we have

$$\mathbb{E}[X] = \sum_{i_g^{(1)}=1}^{n_g} \dots \sum_{i_g^{(n_l)}=1}^{n_g} w_{i_g^{(1)}} \dots w_{i_g^{(n_l)}} X(x_{i_g^{(1)}}^{(1)}, \dots, x_{i_g^{(n_l)}}^{(n_l)}) \gamma(x_{i_g^{(1)}}^{(1)}, \dots, x_{i_g^{(n_l)}}^{(n_l)}). \quad (14)$$

For a quadrature with n_g points in each direction, and using n_l load groups, we need to compute X and γ a total of $n_g^{n_l}$ times. Clearly, this can quickly become very costly.

5.4. Example: Plate. We consider the plate shown in Figure 5.2. The plate dimensions are (all units in mks): $0 \leq x \leq 60$, $0 \leq y \leq 30$, $0 \leq z \leq 0.1$. Density, Young's modulus and Poisson rate were set to $\rho = 7.8$, $E = 2 \cdot 10^9$, $\nu = 0.3$, respectively. The top boundary is clamped ($\mathbf{u} = 0$) and a vertical load is given by $f_y = 4 \cdot 10^5 \xi$, where the scalar ξ lies in $\Xi = (0.8, 1.2)$.

The spatial discretization for the displacement and adjoint is carried out using piecewise linear finite elements. The strength factor is discretized using piecewise constant elements.

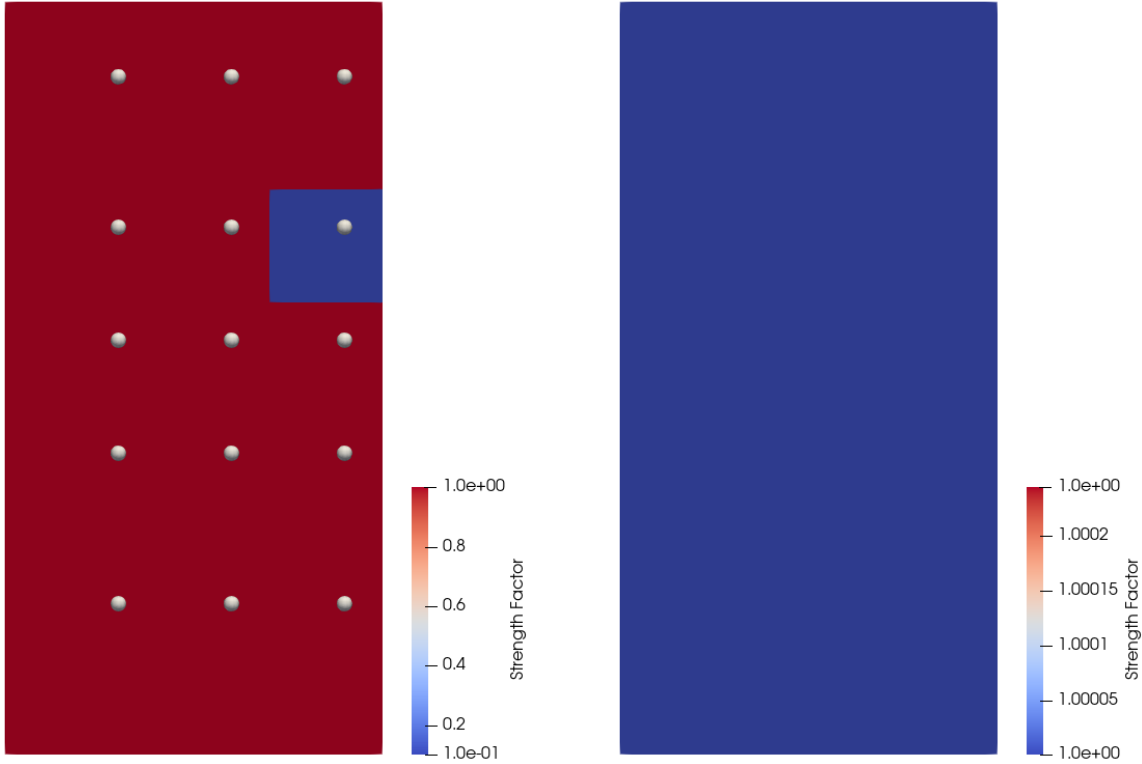


FIGURE 5.2. Left: Target strength factor and sensors. Right: Initial Strength Factor.

Gauss quadrature with 4 terms is used to approximate the integrals over Ξ . Steepest descent with backtracking line search is used as the optimization algorithm. Finally, four smoothing steps are applied to the gradient.

Consider the configuration shown in Figure 5.2 where part of plate has been weakened. The goal is to try to match the displacement corresponding to the configuration shown in this figure.

5.4.1. With Load and Sensor Uncertainty. For each j , the random load is $\hat{f}_y = 10^5 \xi$ where ξ is randomly drawn from a uniform distribution over Ξ . For each j , this gives us the desired measurements \mathbf{u}_j^{md} . That means that every sensor will derive its values from a different load case. Thus, we can see it as having m conflicting realizations of the random variable at the same time.

Figure 5.3 shows a comparison between the standard expectation and CVaR_β with different levels of β . All optimization runs took 100 iterations for a decrease in the objective function of 2 orders of magnitude. Clearly, CVaR_β performs much better as it is able to get rid of the extra weak spot that the uncertainties produced.

It is worth noting that as larger β are utilized, the solution tends to become more under-developed, meaning that the values of the parameter do not go all the way down to 0.1 as we would like. However, this is not a problem since our main goal is to accurately find the location of the weakening and the value placed on it is not as important.

5.4.2. With Load Uncertainty. In this example, we look at high dimensionality in the load uncertainty. For this case, all sensors will measure the same (deterministic) constant load given by $f_y = 4 \cdot 10^5$, applied at the top surface. In our optimization problem, we apply a random load as described below.

In order to properly test a high-dimensional, worst case scenario, we compute the target displacements using a deterministic load with a linear variation $f_y = 4.4 \cdot 10^5 - \frac{8 \cdot 10^4}{60}x$, as shown in Figure 5.4 (top right). This sets up an interesting dimensionality problem, as the load was assumed to be constant, the linear behaviour of this load is not known by the optimizer.

The best one can do if one expects a non-constant variation of the loading in space, is to set up as many load groups as one can afford to in order to best adapt to unforeseen random behaviour. In this example, we choose to divide the loaded surface in 4 groups, each with its own associated random variable. Illustrations of this concept can be seen in the bottom row of figure 5.4.

Using a Gauss quadrature scheme of order 3, our optimization algorithm required 3^4 state solves in order to evaluate the objective function and the same number of adjoint solves to evaluate the gradient during each optimization iteration. Recall that the quadrature is used to approximate the expectation in both the objective function and the gradient with respect to α .

We optimize the same parameters as the previous case, with the difference that our integration limit were now constrained to $\Xi = (0.9, 1.1)$. The results are shown in Figure 5.5, which displays that the risk neutral approach is comparable to CVaR_β for low β . However, the accuracy improves as β gets larger.

5.5. Example: Large Truss Structure Under Load and Sensor Uncertainty. Consider the large truss structure shown in Figure 5.6. Structures such as this one are found in the solar panels of the international space station, or in cranes. The structure is composed of 350 beam elements with transversal area $A = 5\text{cm}^2$. Density, Young's modulus and Poisson

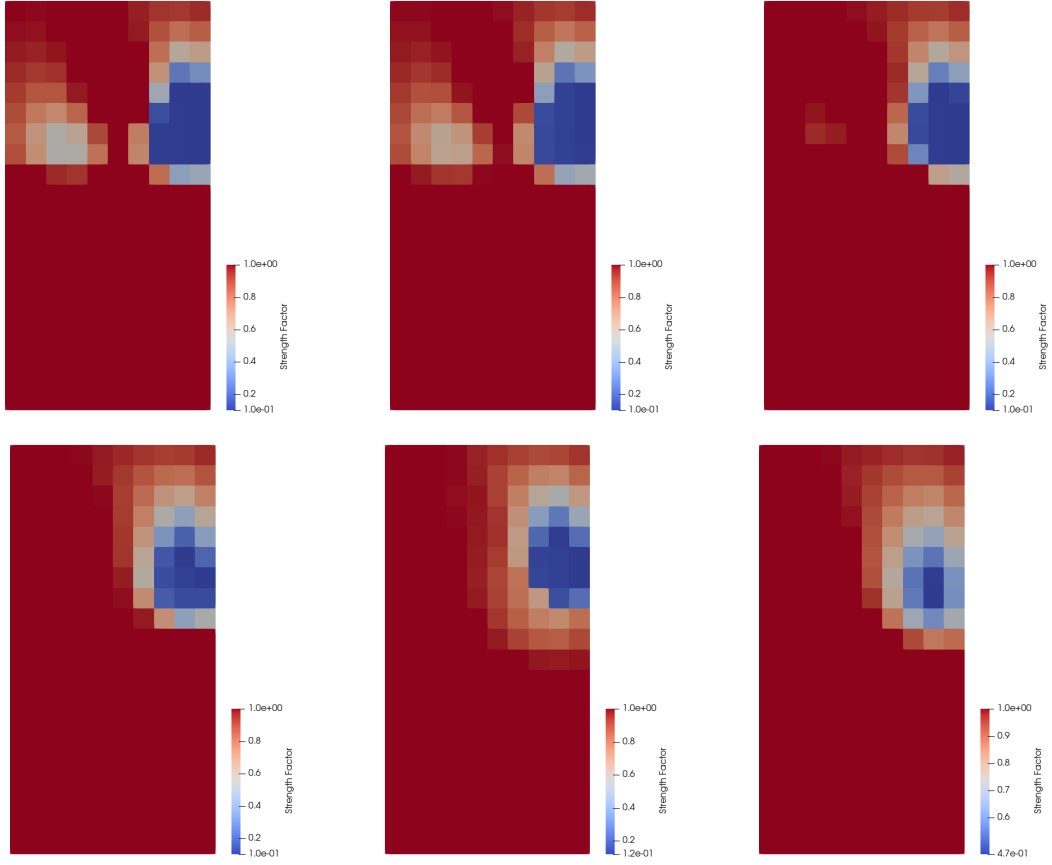


FIGURE 5.3. Top row: first panel (standard expectation); middle and right panels (CVaR_β with $\beta = 0.1$ and 0.3). Bottom row (from left to right): CVaR_β with $\beta = 0.5, 0.7$ and 0.9 . Clearly, CVaR_β performs much better than the standard expectation.

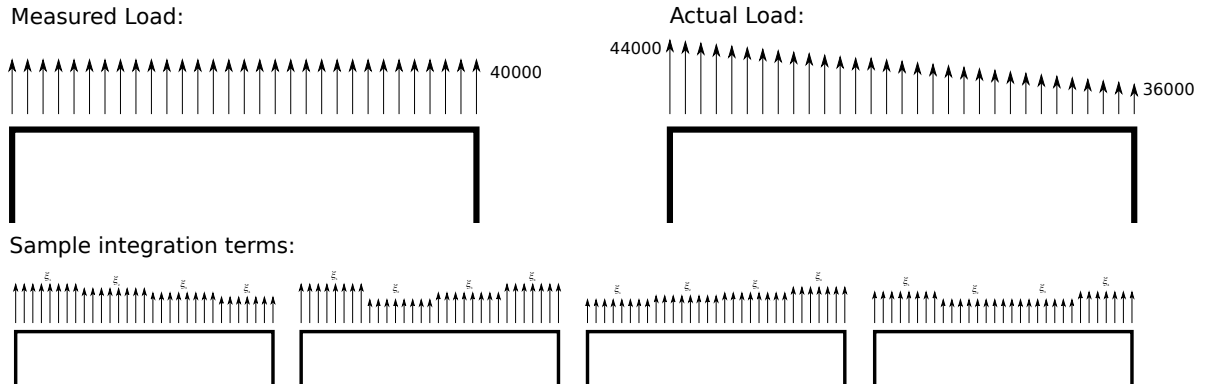


FIGURE 5.4. Top Left: Loading assumed to be present. Top Right: Actual loading used to compute the sensor displacements. Bottom: Examples of loading configurations used in the integration process.

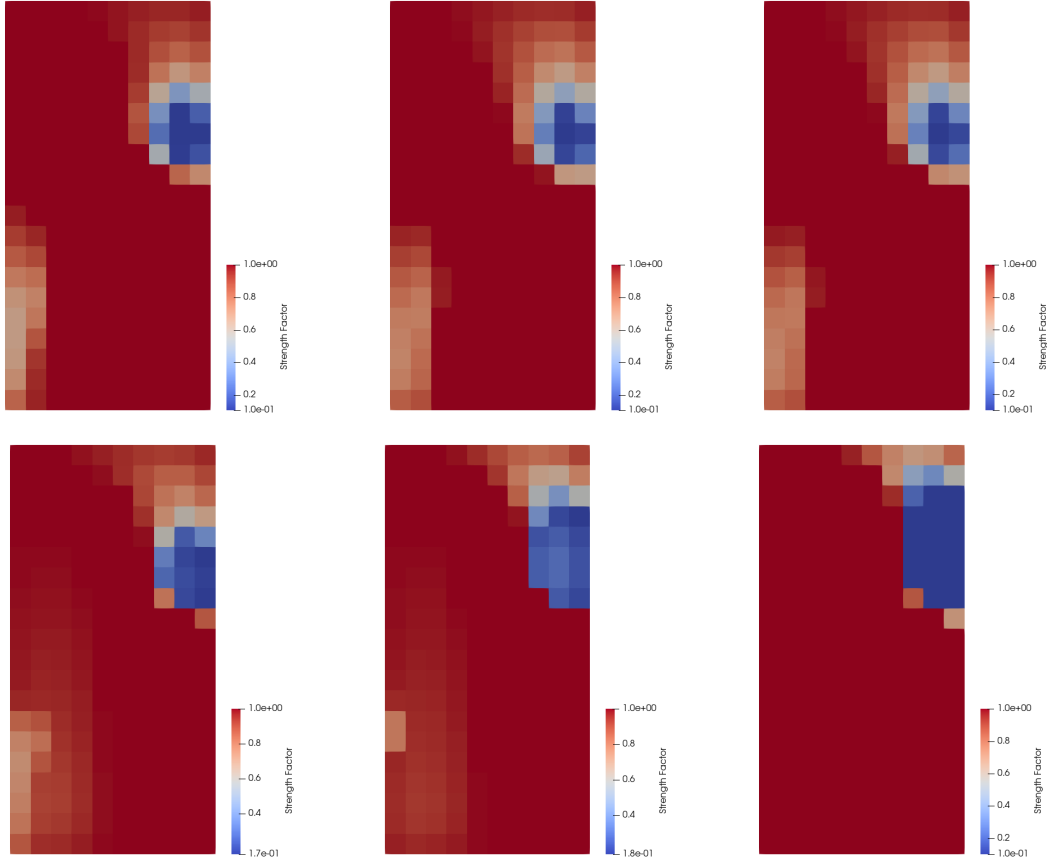


FIGURE 5.5. Top row: first panel (standard expectation); middle and right panels (CVaR_β with $\beta = 0.3$ and 0.5). Bottom row (from left to right): CVaR_β with $\beta = 0.6, 0.7$ and 0.9 . CVaR_β performs better than the standard expectation.

rate were set to $\rho = 7.8$, $E = 2 \cdot 10^9$, $\nu = 0.3$, respectively. Moreover, 6 load cases were set up in order to cover a wide set of scenarios. These are presented in Figure 5.7. The loads on each case were allowed to be scaled by a random variable ξ , where ξ lies in $\Xi = (0.8, 1.2)$.

As in the previous case, the strength factor is discretized using piecewise constant elements. Gauss quadrature with 4 terms is used to approximate the integrals over Ξ . Steepest descent with backtracking line search is used as the optimization algorithm. Four smoothing steps are applied to the gradient.

For each load case, and each measurement point, a new random variable ξ was generated as in the first plate example. Ten sensors were used in this example (cf. Figure 5.6). The weakened configuration was run $\text{n sensor} \cdot \text{n case}$ times in order to compute all the target displacements. Figure 5.8 shows a comparison between the standard expectation and CVaR_β with different levels of β . As in the case of the plate, we again observe significant benefits when using CVaR_β .

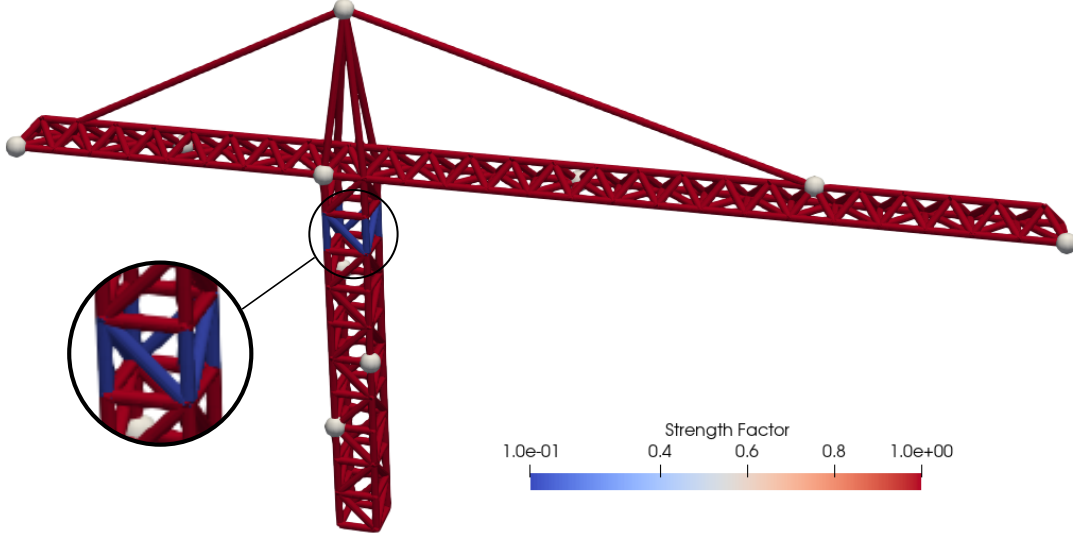


FIGURE 5.6. The goal is to achieve the strength factor shown in this large truss configuration. Notice that several beams on the structure have been weakened.

5.6. Example: Footbridge Under Thermal Loading. This case considers a typical footbridge and was taken from [9], see also [1] for results in the deterministic setting. The different types of trusses and plates whose dimensions have been compiled in Table 5.1, can be discerned from Figure 5.9. Density, Young's modulus and Poisson ratio were set to $\rho = 7,800 \text{ kg/m}^3$, $E = 2 \cdot 10^{11} \text{ kg/sec}^2/\text{m}$, $\nu = 0.3$ respectively. The structure was modeled using 136 shell and 329 beam elements. The bridge is under a distributed load of 1 MPa in the downwards direction, applied to every plate, as well as gravity.

Component #	Shape. Dimensions in mm
1	Steel plate. $t = 10$
2	Steel beam. Hollow section $300 \times 200 \times 12$
3	Steel beam. Hollow section $200 \times 200 \times 10$
4	Steel beam. Hollow section $180 \times 180 \times 10$
5	Steel beam. Hollow section $180 \times 180 \times 5$
6	Steel beam. Hollow section $200 \times 200 \times 10$
7	Steel beam. Hollow section $200 \times 100 \times 5$

TABLE 5.1. Footbridge: Components

In large structures it is typical to have a certain degree of deformation as a result of variations in ambient temperature. This could be a considerable source of uncertainty if this temperature is not correctly accounted for.

In the elasticity equations, a strain component is given by a change in temperature as

$$\epsilon_t = \alpha_{\text{exp}} \Delta T, \quad (15)$$

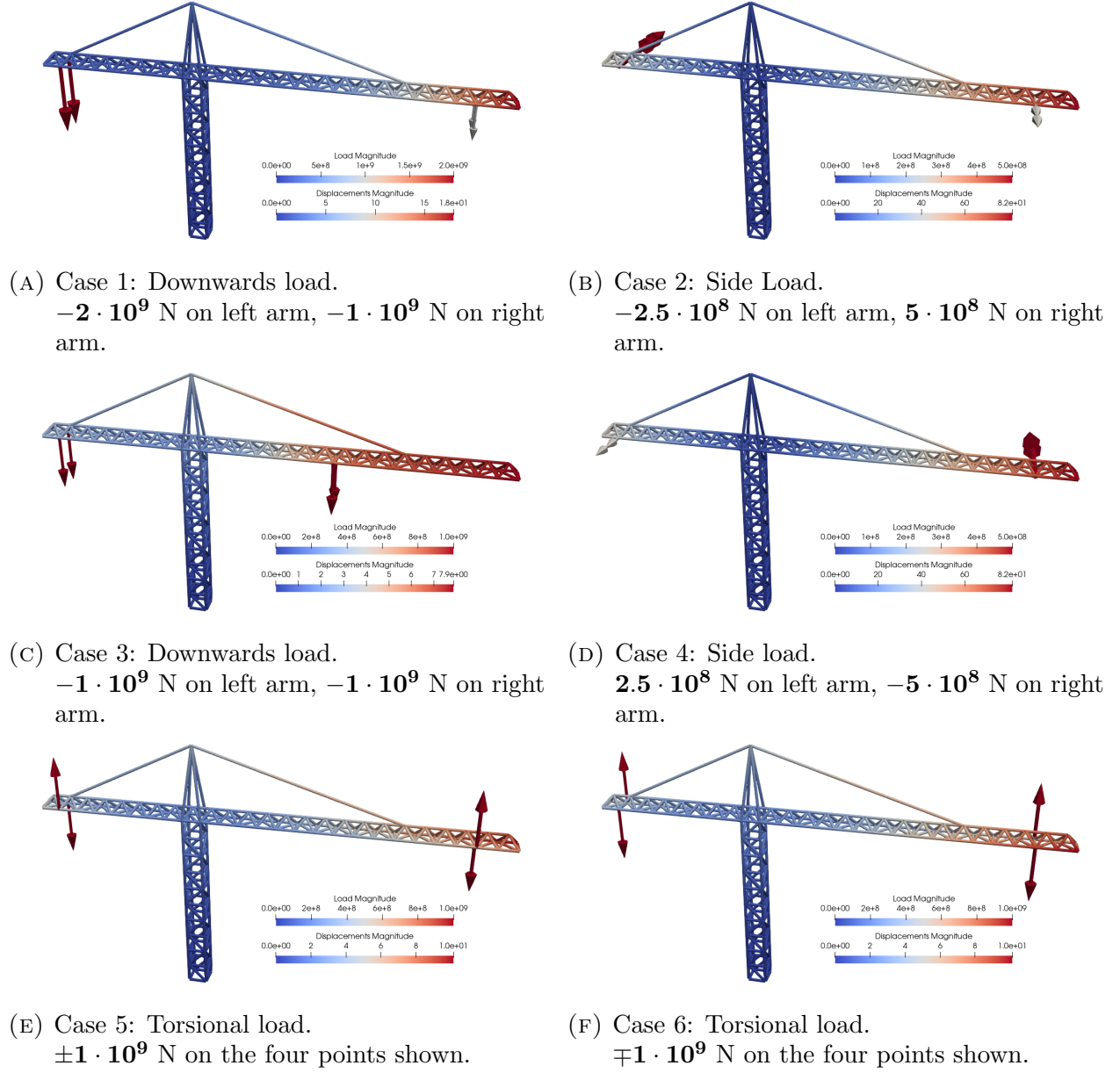


FIGURE 5.7. Load cases run simultaneously for the crane problem.

where α_{exp} is the coefficient of thermal expansion, which for our case is $\alpha_{\text{exp}} = 11 \cdot 10^{-6}$. Naturally, imposing this strain on the constrained system will result in a stress along the structure.

A weakened configuration such as the one shown in Figure 5.10 is solved for the sensor displacements. In this case however, a $\Delta T = -30K$ is imposed on the whole structure for this target configuration. Gauss quadrature with 4 terms is used to approximate the integrals over $\Xi = (0.9, 1.1)$. Steepest descent with backtracking line search is used as the optimization algorithm. Finally, five smoothing steps are applied to the gradient.

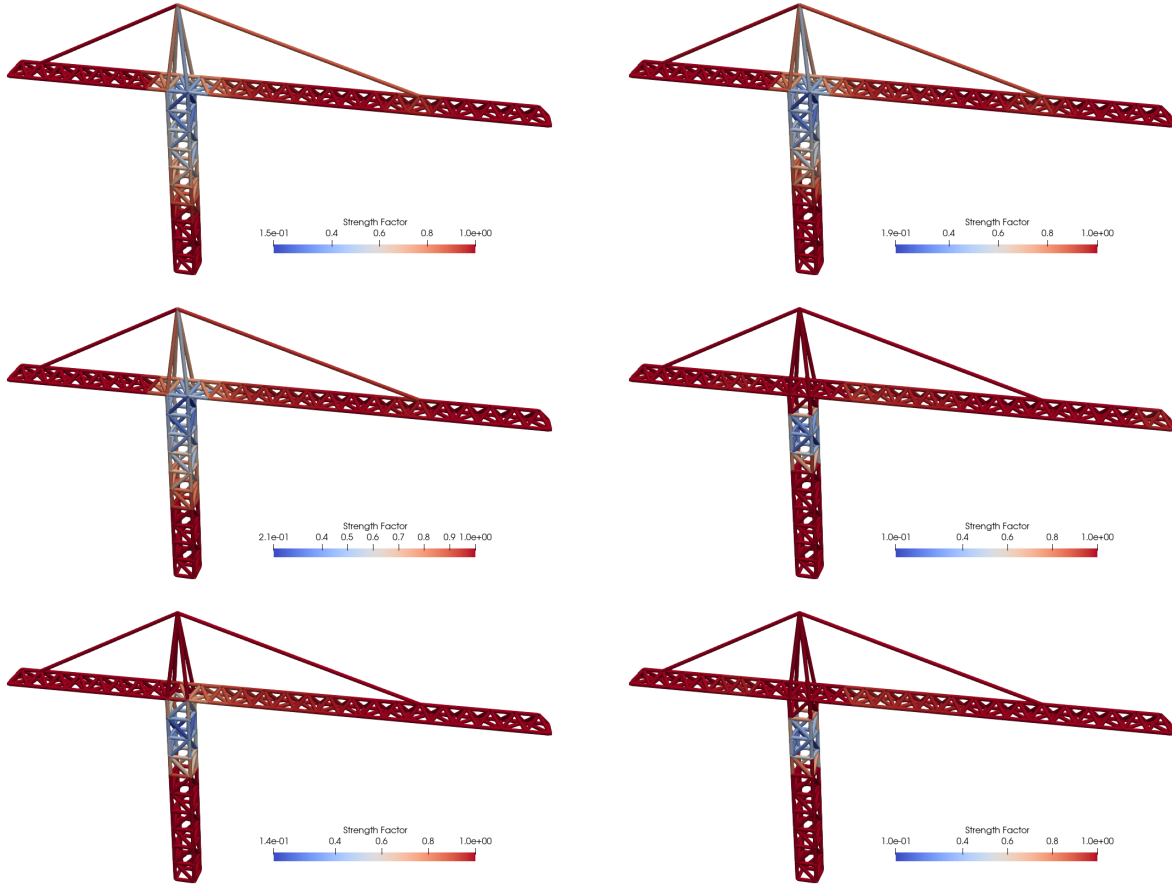


FIGURE 5.8. Top row: left panel (standard expectation); right panel CVaR_β with $\beta = 0.1$. Middle row: CVaR_β with $\beta = 0.3, 0.5$. Bottom row: CVaR_β with $\beta = 0.7, 0.8$. Clearly, CVaR_β performs much better than the standard expectation.

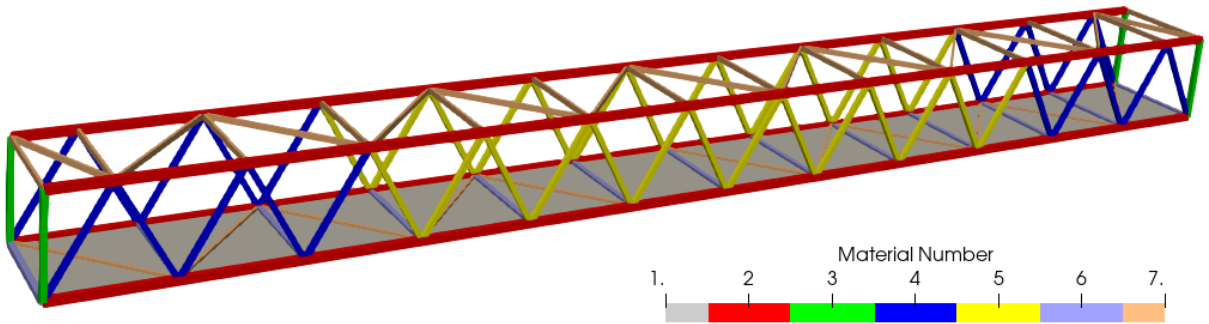


FIGURE 5.9. Footbridge: Components.

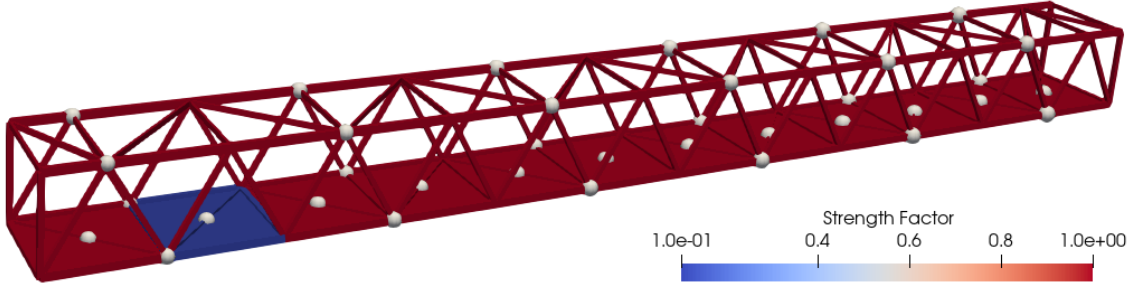


FIGURE 5.10. Footbridge: Target configuration with sensors.

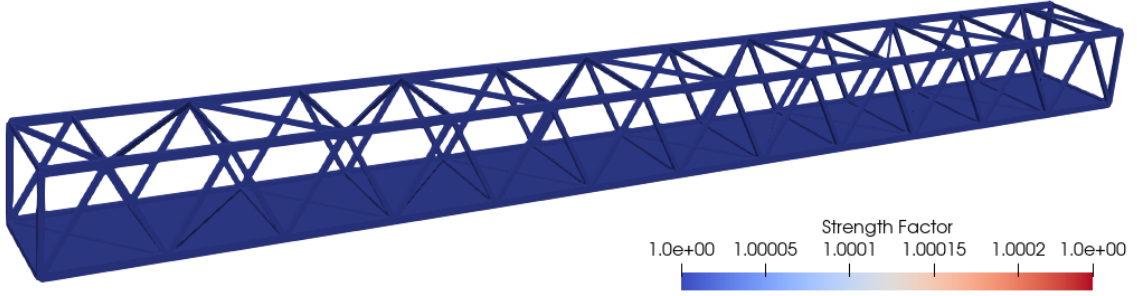


FIGURE 5.11. Footbridge: Initial configuration.

We optimize starting with the configuration from Figure 5.11, in which $\Delta T = \pm 29.8K$ is assumed to be present as our random variable. This value is $\pm 10\%$ of the ambient temperature $T = 298K$.

Results are shown for the risk neutral approach in Figure 5.12 and for a CVaR_β approach with $\beta = 0.3$ in Figure 5.13. Both approaches took around 50 gradient descent iterations for a decrease of 3 order of magnitude in the objective.

It is clear that both methods perform well. The uncertain thermal loading results in a *false positive* of a weak spot on the right side of the structure. While the CVaR_β method is better at suppressing this spot, it also results in a slightly more underdeveloped solution for this case, as can be seen in the color maps.

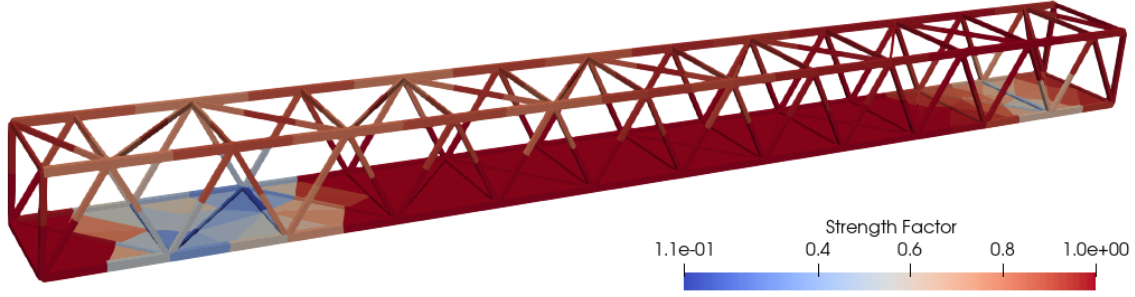


FIGURE 5.12. Footbridge: Optimized configuration using risk neutral objective function

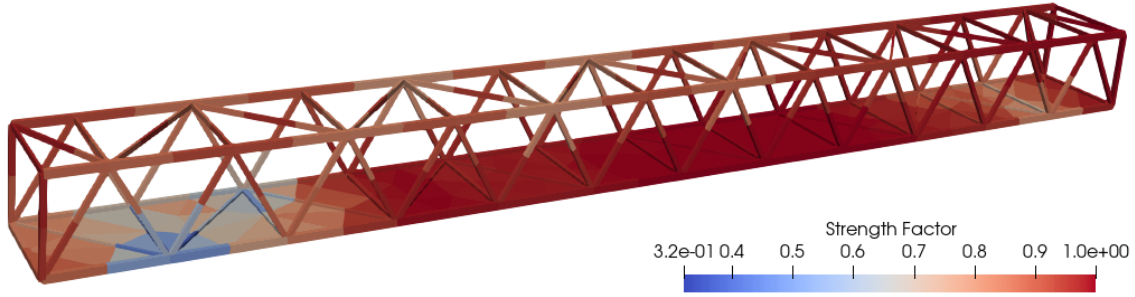


FIGURE 5.13. Footbridge: Optimized configuration using CVaR_β objective function with $\beta = 0.3$.

6. CONCLUSION

This work studies the role of risk-measures in digital-twins to tackle uncertainty in loads and measurements. In particular, the focus is on identifying weaknesses in structures under uncertainty, leading to an optimization problem with PDE constraints. This is also termed as ‘digital twin’ because it takes data from the physical system (using sensors) and supplements appropriate predictions. Risk measures such as CVaR_β are known to be more conservative than risk neutral measures such as expectation and can lead to robust designs which are resilient to rare events.

While the results are very promising, some questions remain unanswered with the use of risk-averse optimization for system identification. As we assume a certain degree of uncertainty on the supposed known loads, and we add more sources of load uncertainty in the shape of thermal or wind loading, the optimization tasks become more complex and costly. The use of a discrete division of the load sources with group loading allows the problems to be tractable, but one could further explore other strategies such as tensor train decomposition [3, 4].

As the numerical results show, the conservativeness of the CVaR_β approach sometimes leads to underdeveloped solutions, which tends not to be a problem for system identification, as the proper location of the weak spots are found. In addition, it was found that the best results were obtained for cases in which a large uncertainty in sensor measurements was present.

ACKNOWLEDGMENTS

This work is partially supported by NSF grants DMS-2110263, the Air Force Office of Scientific Research (AFOSR) under Award NO: FA9550-22-1-0248, and Office of Naval Research (ONR).

REFERENCES

- [1] Facundo N. Airaud, Rainald Löhner, Roland Wüchner, and Harbir Antil. Adjoint-based determination of weaknesses in structures. *Computer Methods in Applied Mechanics and Engineering*, 417:116471, 2023.
- [2] Harbir Antil, Livia Betz, and Daniel Wachsmuth. Strong stationarity for optimal control problems with non-smooth integral equation constraints: Application to a continuous dnn. *Applied Mathematics & Optimization*, 88(3):84, 2023.
- [3] Harbir Antil, Sergey Dolgov, and Akwum Onwunta. Ttrisk: Tensor train decomposition algorithm for risk averse optimization. *Numerical Linear Algebra with Applications*, n/a(n/a):e2481.
- [4] Harbir Antil, Sergey Dolgov, and Akwum Onwunta. State-constrained optimization problems under uncertainty: A tensor train approach. *arXiv preprint arXiv:2301.08684*, 2023.
- [5] Harbir Antil, Drew P. Kouri, Martin-D. Lacasse, and Denis Ridzal, editors. *Frontiers in PDE-constrained optimization*, volume 163 of *The IMA Volumes in Mathematics and its Applications*. Springer, New York, 2018. Papers based on the workshop held at the Institute for Mathematics and its Applications, Minneapolis, MN, June 6–10, 2016.
- [6] Francisco Chinesta, Elias Cueto, Emmanuelle Abisset-Chavanne, Jean Louis Duval, and Fouad El Khaldi. Virtual, digital and hybrid twins: a new paradigm in data-based engineering and engineered data. *Archives of computational methods in engineering*, 27:105–134, 2020.
- [7] Guido Dhondt. Calculix user’s manual version 2.20. *Munich, Germany*, 2022.
- [8] Michael Hinze, René Pinnau, Michael Ulbrich, and Stefan Ulbrich. *Optimization with PDE constraints*, volume 23 of *Mathematical Modelling: Theory and Applications*. Springer, New York, 2009.
- [9] Artūras Kilikevičius, Darius Bačinskis, Jaroslaw Selech, Jonas Matijošius, Kristina Kilikevičienė, Darius Vainorius, Dariusz Ulbrich, and Dawid Romek. The influence of different loads on the footbridge dynamic parameters. *Symmetry*, 12(4):657, 2020.
- [10] D. P. Kouri and T. M. Surowiec. Risk-averse PDE-constrained optimization using the conditional value-at-risk. *SIAM J. Optim.*, 26(1):365–396, 2016.
- [11] Jacques-L. Lions. *Optimal control of systems governed by partial differential equations*. Translated from the French by S. K. Mitter. Die Grundlehren der mathematischen Wissenschaften, Band 170. Springer-Verlag, New York-Berlin, 1971.
- [12] Laura Mainini and Karen Willcox. Surrogate modeling approach to support real-time structural assessment and decision making. *AIAA Journal*, 53(6):1612–1626, 2015.
- [13] R Tyrrell Rockafellar and Stanislav Uryasev. Optimization of conditional value-at-risk. *Journal of risk*, 2:21–42, 2000.
- [14] R Tyrrell Rockafellar and Stanislav Uryasev. Conditional value-at-risk for general loss distributions. *Journal of banking & finance*, 26(7):1443–1471, 2002.
- [15] Alexander Shapiro, Darinka Dentcheva, and Andrzej Ruszczyński. *Lectures on stochastic programming*, volume 9 of *MOS-SIAM Series on Optimization*. SIAM, Philadelphia, PA; MOS, Philadelphia, PA, second edition, 2014. Modeling and theory.

- [16] Juan C Simo and Thomas JR Hughes. *Computational inelasticity*, volume 7. Springer Science & Business Media, 2006.
- [17] Fredi Tröltzsch. *Optimal control of partial differential equations*, volume 112 of *Graduate Studies in Mathematics*. American Mathematical Society, Providence, RI, 2010. Theory, methods and applications, Translated from the 2005 German original by Jürgen Sprekels.
- [18] Michael Ulbrich. *Semismooth Newton methods for variational inequalities and constrained optimization problems in function spaces*, volume 11 of *MOS-SIAM Series on Optimization*. Society for Industrial and Applied Mathematics (SIAM), Philadelphia, PA; Mathematical Optimization Society, Philadelphia, PA, 2011.
- [19] Olek C Zienkiewicz, Robert Leroy Taylor, and Jian Z Zhu. *The finite element method: its basis and fundamentals*. Elsevier, 2005.

CENTER FOR COMPUTATIONAL FLUID DYNAMICS AND DEPARTMENT OF PHYSICS AND ASTRONOMY,
GEORGE MASON UNIVERSITY, FAIRFAX, VA 22030, USA.

Email address: fairaudo@gmu.edu

CENTER FOR MATHEMATICS AND ARTIFICIAL INTELLIGENCE (CMAI) AND DEPARTMENT OF MATHEMATICAL SCIENCES, GEORGE MASON UNIVERSITY, FAIRFAX, VA 22030, USA.

Email address: hantil@gmu.edu

CENTER FOR COMPUTATIONAL FLUID DYNAMICS AND DEPARTMENT OF PHYSICS AND ASTRONOMY,
GEORGE MASON UNIVERSITY, FAIRFAX, VA 22030, USA.

Email address: rlohner@gmu.edu

CENTER FOR MATHEMATICS AND ARTIFICIAL INTELLIGENCE (CMAI) AND DEPARTMENT OF MATHEMATICAL SCIENCES, GEORGE MASON UNIVERSITY, FAIRFAX, VA 22030, USA.

Email address: urakhimov@gmu.edu